Chemical Looping Partial Oxidation of Methane: Reducing Carbon Deposition through Alloying

Journal Article

Author(s):
Donat, Felix; Kierzkowska, Agnieszka; Müller, Christoph R.

Publication date:
2022-09-01

Permanent link:
https://doi.org/10.3929/ethz-b-000560507

Originally published in:
Energy & Fuels 36(17), https://doi.org/10.1021/acs.energyfuels.2c01345

Funding acknowledgement:
819573 - Advancing CO2 Capture Materials by Atomic Scale Design: the Quest for Understanding (EC)
180544 - NCCR Catalysis (phase I) (SNF)

Chemical looping partial oxidation of methane: Reducing carbon deposition through alloying

*Felix Donat, Agnieszka Kierzkowska, Christoph R. Müller**

Laboratory of Energy Science and Engineering, Department of Mechanical and Process Engineering, ETH Zurich, Leonhardstrasse 21, 8092 Zürich, Switzerland

KEYWORDS: chemical looping; oxygen carrier; carbon deposition; partial oxidation; alloy

ABSTRACT. In chemical looping, Fe-containing oxygen carriers can catalyze as a side reaction the decomposition of methane, which results in the deposition of carbon on their surface with multiple adverse effects. In this work, we propose a strategy to reduce the extent of carbon deposition by using Co as a second redox-active metal that forms a bimetallic phase with Fe during reduction. We show for a perovskite-based oxygen carrier that the formation of the bimetallic Fe-Co phase improves the dispersion and decreases the size of iron within the material, which may influence its catalytic effect on the decomposition of methane (in addition to potential changes in its electronic structure).

Chemical looping describes a set of metal oxide-mediated redox reactions, in which, in their original form, gaseous or solid fuels are combusted to generate heat without CO_2 emissions into the atmosphere [1,2]. This is possible because the combustion reaction is split into two half-steps: The reduction step during which the fuel is fully oxidized (to carbon dioxide and steam) by the lattice oxygen of the metal oxide, and the oxidation step during which the reduced metal oxide is re-oxidized by the oxygen contained in air. The gas environments of the two reaction steps are temporally or spatially separated, resulting in an

unmixed combustion process from which carbon dioxide of high purity can readily be obtained [3]. Chemical looping has come into prominence in the early 2000s through the research activities of Prof. Lyngfelt and his co-workers [4–8], which has led to a remarkable boost in the advancement of high-temperature redox materials (oxygen carriers) [9,10] and reactor technologies (e.g. interconnected fluidized beds involving particle transfer) [11,12].

Depending on the type of metal oxide used as the oxygen carrier and its thermodynamic properties (i.e. the equilibrium partial pressure of oxygen, $p_{O2,eq}$) when transitioning between two oxidation states at a certain temperature, the chemical looping scheme can be applied to many different conversion reactions and applications [13,14]. Examples include air separation (when the $p_{O2,eq}$ is very high, > 10^{-1} bar) [15,16] or the partial oxidation of methane to syngas (when the $p_{O2,eq}$ is very low, ≈ 10^{-20} bar) [17,18]. Oxygen carriers that partially oxidize methane to syngas (a mixture of hydrogen and carbon monoxide) at very high selectivity enable also the efficient splitting of water (to form hydrogen) or carbon dioxide (to form carbon monoxide), such that both the reduction and the oxidation of the oxygen carrier yield valuable products [19]. La-Fe-based perovskites are particularly suited as oxygen carriers for the chemical looping-based partial oxidation of methane (CL-POX), and many studies have reported selectivities > 90 % towards carbon monoxide with hydrogen to carbon monoxide ratios of ca. two [20–22]. Based on density functional theory (DFT) calculations and experimental results, Jiang et al. found that lanthanum enables higher syngas yields than other A-site lanthanides due to the lowest charge-transfer energy (a descriptor to quantify the degree of Fe-O covalency in the perovskite) [23]. However, iron, the redox-active component of the oxygen carrier in the B-site of La-Fe-based perovskites, is potentially problematic for a scheme in which pure hydrogen is to be produced during the oxidation step (besides syngas during the reduction step). This is because iron catalyzes the decomposition of methane ($CH_4 \rightarrow 2\ H_2 + C$) [24–26], resulting in the deposition of carbon on the surface of the oxygen carrier; the carbon will then be gasified by steam in the oxidation step, thereby contaminating the hydrogen produced. Carbon deposition is usually observed when La-Fe-based perovskites are reduced by methane [27,28], but can be prevented by limiting the extent of the reduction of the oxygen carrier such that only a small fraction of the redox-active lattice oxygen is

utilized [29,30], e.g. by reducing iron partially from $Fe^{3+/4+}$ to Fe^{2+} instead of Fe^0. This, of course, lowers the useable oxygen storage capacity (OSC) of the oxygen carrier, which, on a process level, would require greater amounts of oxygen carrier to obtain a certain amount of product gases. Furthermore, carbon deposition may impair the mechanical stability of the oxygen carrier, and so several strategies have been proposed to avoid carbon deposition during the reduction of La-Fe-based oxygen carriers with methane. For example, Zhang et al. showed that through distorting FeO_6 octahedra in $La_{1-x}Ce_xFeO_3$, the bulk oxygen mobility in the perovskite was enhanced, which in turn reduced carbon deposition; the effect was most significant for x=0.5 [28]. For $La_xCe_{1-x}Fe_xNi_{1-x}O_3$, Yuan et al. claimed that carbon deposition was caused predominantly by Ni species, and optimizing both the calcination temperature (to 800 °C) and the ratio of Fe:Ni (to 1.5) in the oxygen carrier decreased carbon deposition significantly [31]. Imtiaz et al. suggested that adding Cu to Fe-based oxygen carriers partially covers Fe and thereby reduces its catalytic activity for the decomposition of methane [32]. However, too large amounts of Cu in the oxygen carrier decrease the yield of hydrogen and potentially accelerate sintering problems. Zhang et al. proposed to use Sn as a promoter in $BaFe_{1-x}Sn_xO_3$ to improve both the oxygen storage capacity and the resistance towards carbon deposition [33]. The material's performance was investigated only in the reduction step (i.e. the partial oxidation step) and the formation of an iron-tin alloy instead of metallic iron during reduction was proposed to suppress the methane decomposition. Although not observed by the authors, using tin as a promoter may be problematic in oxygen carriers for high-temperature applications due to its low melting temperature; further, tin itself may not maintain a high redox activity over multiple cycles.

Here, we show that the addition of a second redox-active metal oxide (i.e. Co-oxide) in a La-Fe-based perovskite reduces the extent of carbon deposition during the reduction step significantly, enabling a greater amount of lattice oxygen to be utilized to produce syngas and pure hydrogen when using steam as the oxidant. Based on our previous works on CL-POX [19,34], we chose $La_{0.8}Sr_{0.2}Fe_{0.95}Al_{0.05}O_3$ as the reference material, and partially substituted Fe with Co to obtain an oxygen carrier with the nominal composition $La_{0.8}Sr_{0.2}Fe_{0.75}Co_{0.2}Al_{0.05}O_3$. Both materials were synthesized from metal nitrates using a protocol reported elsewhere [35], followed by calcination in air at 1200 °C for 12 h. In all experiments and

analyses, fine powder (< 50 μm) was used. X-ray diffraction analysis (PANalytical Empyrean), Figure 1a, shows that pure perovskites were obtained with no other metal oxide phases detected. The elemental composition of the two oxygen carriers was determined experimentally by inductively coupled plasma optical emission spectroscopy (ICP-OES, Agilent 5100 VDV), and it was in good agreement with the nominal composition based on the amounts of metal nitrates used in the synthesis (Figure 1b). The thermodynamic analysis in Figure 1c shows that the decomposition of methane is favored at high temperature; thus, 900 °C was selected as the reaction temperature for the CL-POX process to illustrate the beneficial effect of including Co in the oxygen carrier to reduce carbon deposition. The CL-POX reactions were carried out in a thermogravimetric analyzer (TGA, Mettler Toledo TGA/DSC 3 HT) in two different ways: The oxygen carriers (ca. 30 mg) were always exposed to methane in the reduction step, but the oxidation step was performed either in air (to assess the cyclic stability) or carbon dioxide (to assess the carbon dioxide splitting ability relevant to the CL-POX scheme); note that steam could not be used as the oxidant in the TGA, but possesses a similar oxidation potential as carbon dioxide at 900 °C. Figure 1d shows that both oxygen carriers had a stable redox performance over five reaction cycles. Inspecting an entire redox cycle in detail, Figure 1e reveals a distinct increase in sample weight of $La_{0.8}Sr_{0.2}Fe_{0.95}Al_{0.05}O_3$ during the reduction step due to carbon deposition. In contrast, there was hardly any increase in sample weight of $La_{0.8}Sr_{0.2}Fe_{0.75}Co_{0.2}Al_{0.05}O_3$ after its redox-active lattice oxygen had been removed ($Fe^{3+/4+} \rightarrow Fe^0$ and $Co^{2+/3+} \rightarrow Co^0$), indicating that carbon deposition was negligible. The oxygen carrier without Co reduced at a faster rate, as can be seen when comparing the slopes of the sample mass curves. Analysis of the reduced materials (after 20 min of reduction in methane at 900 °C) through Raman spectroscopy (Thermo Scientific DXR Raman microscope; laser wavelength 532 nm) in Figure 1f confirms that carbon deposition occurred during reduction only for $La_{0.8}Sr_{0.2}Fe_{0.95}Al_{0.05}O_3$ but not for $La_{0.8}Sr_{0.2}Fe_{0.75}Co_{0.2}Al_{0.05}O_3$. If steam was used to re-oxidize the oxygen carrier, pure hydrogen would have been produced.

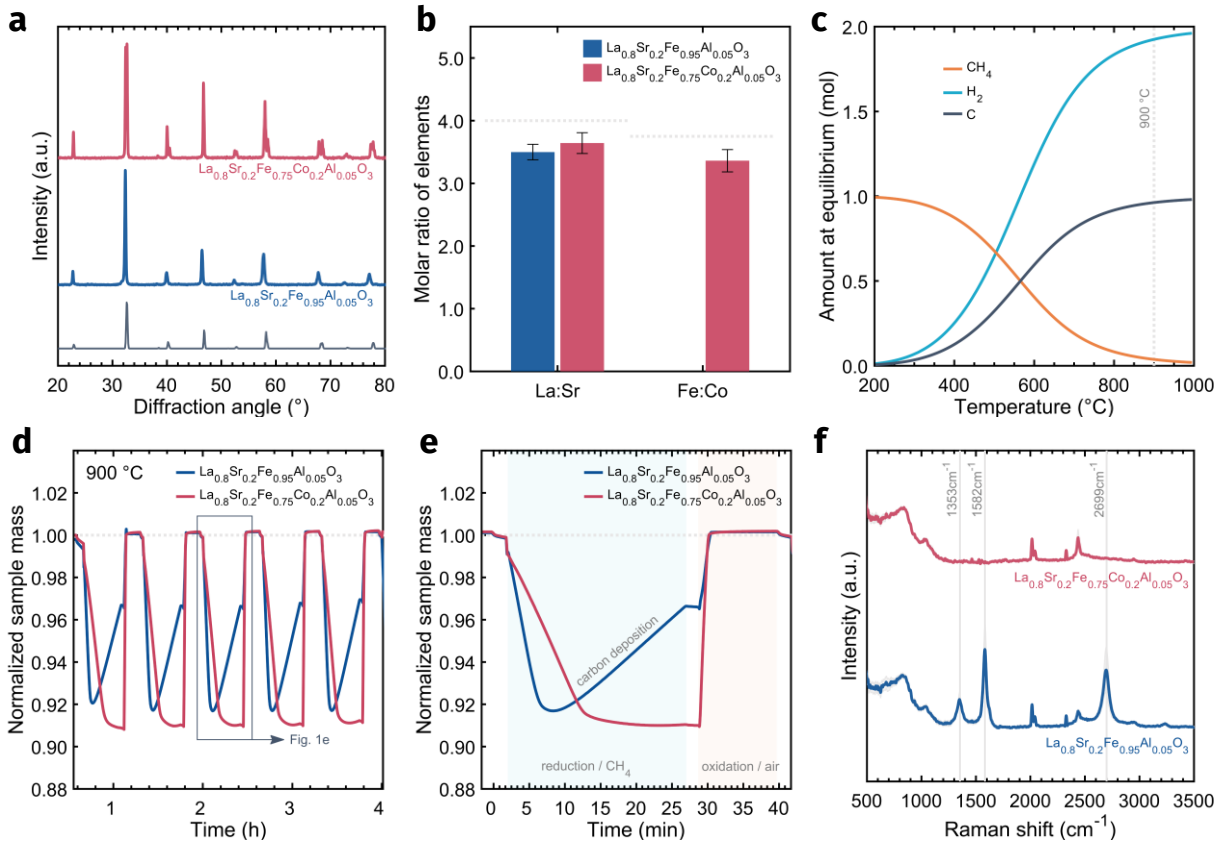

Figure 1: (a) XRD patterns of the as-synthesized oxygen carriers; the gray reference pattern indicates a rhombohedral structure (ICSD collection code 112497). (b) Elemental composition of the as-synthesized oxygen carriers, as determined by ICP-OES. (c) Thermodynamic equilibrium calculations by minimizing the Gibbs free energy of a system containing the species CH_4, CO, CO_2, H_2, H_2O and solid C. (d) Normalized sample mass of the oxygen carriers when cycling them in a TGA (reduction for 25 min in ca. 7 % CH_4/N_2, oxidation for 11 min in air). (e) Magnification of the third redox cycle shown in (d). (f) Raman spectroscopy measurements of the reduced oxygen carriers (TGA, 900 °C, 20 min, ca. 7 % CH_4/N_2). The spectra were averaged based on at least eight separate measurements of different areas of the oxygen carrier particles. The vertical gray lines denote the D, G and 2D bands that are characteristic for carbon species.

In the second series of TGA measurements, the oxygen carriers were re-oxidized by carbon dioxide (Figure 2a). The reduction time was limited to 3 min to ensure no carbon deposition took place for either

of the oxygen carriers (note that the constant increase in sample mass after the reduction step was due to the re-oxidation of the oxygen carriers with oxygen contained in nitrogen and the unavoidable leaking of very small quantities of air into the TGA, in total ca. 80 ppm). The off-gas from the TGA was analyzed (ABB EL3020 gas analyzers) to derive CL-POX performance indicators that are summarized in Figure 2b. The average ratio of hydrogen to carbon monoxide was slightly lower than two, as observed by us previously for a similar La-Fe-based perovskite [19]. The selectivity towards syngas, determined at ca. 20 % of lattice oxygen conversion (defined as the relative mass loss of the oxygen carrier during reduction divided by its oxygen storage capacity), was unity for both oxygen carriers, as there was no production of carbon dioxide and solid carbon. Interestingly, while the total OSC (OSC_{tot}, determined by reduction in hydrogen) was slightly higher for $La_{0.8}Sr_{0.2}Fe_{0.75}Co_{0.2}Al_{0.05}O_3$ than for $La_{0.8}Sr_{0.2}Fe_{0.95}Al_{0.05}O_3$ (10.3 % vs. 9.7 %), the fraction of redox-active lattice oxygen that can be replenished by carbon dioxide or steam (OSC_{CO2}) was lower for $La_{0.8}Sr_{0.2}Fe_{0.75}Co_{0.2}Al_{0.05}O_3$ (87 % vs. 96 %, see also the arrows in Figure 2a at the end of the oxidation step with carbon dioxide). This implies that the thermodynamic properties of the oxygen carrier were altered by the inclusion of Co in the material, and its ability to split carbon dioxide or steam was reduced. Preliminary results using oxygen carriers that had different ratios of Fe:Co indicate that the amount of Co in the material should be relatively low to regenerate a large fraction of the lattice oxygen by carbon dioxide or steam, similar to observations made elsewhere [36].

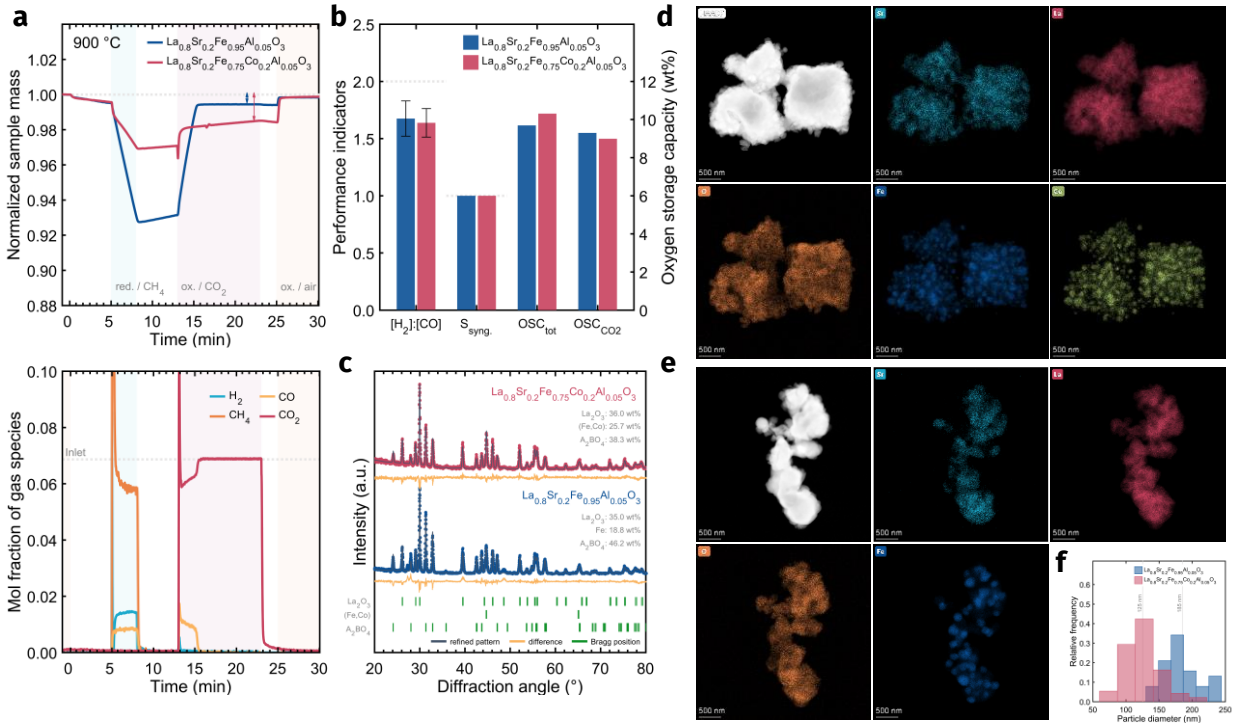

Figure 2: (a) Top: Normalized sample mass of the oxygen carriers when cycling them in a TGA (reduction for 3 min in ca. 7 % CH_4/N_2, oxidation for 10 min in ca. 7 % CO_2, oxidation for 5 min in air). Bottom: Corresponding off-gas profile for $La_{0.8}Sr_{0.2}Fe_{0.95}Al_{0.05}O_3$. (b) Performance indicators of the oxygen carriers during reduction (average ratio H_2:CO, and selectivity towards syngas), and oxygen storage capacities. (c) XRD patterns and Rietveld refinement of the completely reduced oxygen carriers (reduction in ca. 7 % H_2/N_2 at 1000 °C for 10 h). (d) and (e) HAADF images and EDX maps of the completely reduced oxygen carriers ($La_{0.8}Sr_{0.2}Fe_{0.75}Co_{0.2}Al_{0.05}O_3$ and $La_{0.8}Sr_{0.2}Fe_{0.95}Al_{0.05}O_3$) corresponding to the XRD patterns shown in (c). (f) Size distribution of the Fe/Co and Fe particles shown in the EDX maps in (d) and (e); ImageJ was used for the analysis and the individual particle areas were converted into circular equivalent diameters.

XRD analysis and Rietveld refinements of the two completely reduced oxygen carriers (reduction in hydrogen instead of methane) show that their principal phase composition did not differ significantly (Figure 2c). Most of the La was contained in La_2O_3, whereas all Sr, Al and some of the La and Fe formed a non-reducible oxide phase that was fitted with a tetragonal structure (space group I4/mmm, ICSD

collection code 97499, A_2BO_4 in Figure 2c). For $La_{0.8}Sr_{0.2}Fe_{0.75}Co_{0.2}Al_{0.05}O_3$, Fe and Co formed a bimetallic phase, as expected from the Fe-Co phase diagram [37]. In the context of solid oxide fuel cells and the dry reforming of methane, bimetallics with Co have been reported to possess superior resistance towards carbon deposition than their monometallic counterparts [38–41]. In these applications only a fraction of the redox-active lattice is consumed, providing always oxidative species that would prevent carbon from being formed. To better understand the differences of the two completely reduced oxygen carriers in their resistivity towards carbon deposition, scanning transmission electron microscopy (STEM, FEI Talos F200X) was used. From the corresponding energy-dispersive X-ray spectroscopy (EDX) maps in Figure 2d and 2e, the elements La, Sr and O were distributed uniformly in both oxygen carriers (Al is not shown). Remarkably, in $La_{0.8}Sr_{0.2}Fe_{0.95}Al_{0.05}O_3$ large aggregates of Fe were formed (185 ± 28 nm), whereas in $La_{0.8}Sr_{0.2}Fe_{0.75}Co_{0.2}Al_{0.05}O_3$ the aggregates (consisting now of Fe and Co) were much smaller (125 ± 27 nm), see histogram in Figure 2f. We speculate that the presence of Co and the formation of a bimetallic Fe-Co phase contributed to the decrease of the Fe aggregate size during the reduction step and thereby improved their dispersion. Whether this also enabled a better resistance towards carbon deposition for this oxygen carrier is not entirely clear; the smaller size of the Fe-Co particles compared to the Fe agglomerates in the reduced $La_{0.8}Sr_{0.2}Fe_{0.95}Al_{0.05}O_3$ suggests they were more evenly embedded within the material in the vicinity of oxygen-containing phases (although these phases are not reducible), as observed previously for similar perovskite compositions [18,42]. Through the inclusion of Co into the oxygen carrier, the extent of reduction before carbon deposition occurs can be increased significantly (from ca. 70 % for $La_{0.8}Sr_{0.2}Fe_{0.95}Al_{0.05}O_3$). We believe that the addition of redox-active metal oxides that can form solid solutions/alloys with Fe is a viable approach to address the problem of carbon deposition when methane is used as the reductant for Fe-containing oxygen carriers (such as in CL-POX) and large lattice oxygen utilization is envisaged. More detailed studies should investigate whether the effect on the reduction of carbon deposition is sustained over a larger number of redox cycles. Further, the changes in the oxygen carrier's geometrical and electronic structure when a second redox-active species is included in a certain stoichiometry should be examined, e.g. using pair distribution function (PDF) analysis from

total scattering data or X-ray absorption spectroscopy (XAS). Our preliminary, ongoing studies indicate that the extend of carbon deposition depends also on the ratio La:Sr or Fe:Co, suggesting the influence of the bimetallic Fe-Co phase on its catalytic properties for the decomposition of methane reaches beyond a particle size effect.

AUTHOR INFORMATION

Corresponding author: Prof. Christoph R. Müller, email: muelchri@ethz.ch

ACKNOWLEDGMENT

Christoph R. Müller acknowledges funding by the European Research Council (ERC) under the European Union's Horizon 2020 research and innovation program under grant agreement no. 819573. This publication was created as part of NCCR Catalysis (grant number 180544), a National Centre of Competence in Research funded by the Swiss National Science Foundation.

REFERENCES

(1) Ishida, M.; Jin, H. A New Advanced Power-Generation System Using Chemical-Looping Combustion. *Energy* **1994**, *19*, 415–422.

(2) Jin, H.; Okamoto, T.; Ishida, M. Development of a Novel Chemical-Looping Combustion: Synthesis of a Solid Looping Material of NiO/NiAl2O4. *Ind. Eng. Chem. Res.* **1999**, *38*, 126–132.

(3) Lyon, R. K.; Cole, J. A. Unmixed Combustion: An Alternative to Fire. *Combust. Flame* **2000**, *121*, 249–261.

(4) Lyngfelt, A.; Leckner, B.; Mattisson, T. A Fluidized-Bed Combustion Process with Inherent CO2 Separation; Application of Chemical-Looping Combustion. *Chem. Eng. Sci.* **2001**, *56*, 3101–3113.

(5) Cho, P.; Mattisson, T.; Lyngfelt, A. Comparison of Iron-, Nickel-, Copper- and Manganese-Based Oxygen Carriers for Chemical-Looping Combustion. *Fuel* **2004**, *83*, 1215–1225.

(6) Mattisson, T.; Johansson, M.; Lyngfelt, A. Multicycle Reduction and Oxidation of Different Types Chemical-Looping Combustion. *Energy & Fuels* **2004**, *18*, 628–637.

(7) Mattisson, T.; Järdnäs, A.; Lyngfelt, A. Reactivity of Some Metal Oxides Supported on Alumina with Alternating Methane and Oxygen - Application for Chemical-Looping Combustion. *Energy and Fuels* **2003**, *17*, 643–651.

(8) Mattisson, T.; Lyngfelt, A.; Cho, P. The Use of Iron Oxide as an Oxygen Carrier in Chemical-Looping Combustion of Methane with Inherent Separation of CO2. *Fuel* **2001**, *80*, 1953–1962.

(9) Adanez, J.; Abad, A.; Garcia-Labiano, F.; Gayan, P.; Diego, L. F. Progress in Chemical-Looping Combustion and Reforming Technologies. *Prog. Energy Combust. Sci.* **2012**, *38*, 215–282.

(10) Qasim, M.; Ayoub, M.; Ghazali, N. A.; Aqsha, A.; Ameen, M. Recent Advances and Development of Various Oxygen Carriers for the Chemical Looping Combustion Process: A Review. *Ind. Eng. Chem. Res.* **2021**, *60*, 8621–8641.

(11) Mattisson, T.; Keller, M.; Linderholm, C.; Moldenhauer, P.; Rydén, M.; Leion, H.; Lyngfelt, A. Chemical-Looping Technologies Using Circulating Fluidized Bed Systems: Status of Development. *Fuel Process. Technol.* **2018**, *172*, 1–12.

(12) Lyngfelt, A.; Pallarès, D.; Linderholm, C.; Lind, F.; Thunman, H.; Leckner, B. Achieving Adequate Circulation in Chemical Looping Combustion─Design Proposal for a 200 MWth Chemical Looping Combustion Circulating Fluidized Bed Boiler. *Energy and Fuels* **2021**.

(13) Wang, X.; Gao, Y.; Krzystowczyk, E.; Iftikhar, S.; Dou, J.; Cai, R.; Wang, H.; Ruan, C.; Ye, S.; Li, F. High-Throughput Oxygen Chemical Potential Engineering of Perovskite Oxides for Chemical Looping Applications. *Energy Environ. Sci.* **2022**, *15*, 1512-1528.

(14) Zhu, X.; Imtiaz, Q.; Donat, F.; Müller, C. R.; Li, F. Chemical Looping beyond Combustion-a Perspective. *Energy Environ. Sci.* **2020**, *13*, 772–804.

(15) Krzystowczyk, E.; Haribal, V.; Dou, J.; Li, F. Chemical Looping Air Separation Using a Perovskite-Based Oxygen Sorbent: System Design and Process Analysis. *ACS Sustain. Chem. Eng.* **2021**, *9*, 12185–12195.

(16) Görke, R. H.; Marek, E. J.; Donat, F.; Scott, S. A. Reduction and Oxidation Behavior of Strontium Perovskites for Chemical Looping Air Separation. *Int. J. Greenh. Gas Control* **2020**, *94*, 102891.

(17) Liu, Y.; Qin, L.; Cheng, Z.; Goetze, J. W.; Kong, F.; Fan, J. A.; Fan, L.-S. Near 100% CO Selectivity in Nanoscaled Iron-Based Oxygen Carriers for Chemical Looping Methane Partial Oxidation. *Nat. Commun.* **2019**, *10*, 5503.

(18) Zhang, L.; Xu, W.; Wu, J.; Hu, Y.; Huang, C.; Zhu, Y.; Tian, M.; Kang, Y.; Pan, X.; Su, Y.; et al. Identifying the Role of A-Site Cations in Modulating Oxygen Capacity of Iron-Based Perovskite for Enhanced Chemical Looping Methane-to-Syngas Conversion. *ACS Catal.* **2020**, *10*, 9420–9430.

(19) Donat, F.; Xu, Y.; Müller, C. R. Combined Partial Oxidation of Methane to Synthesis Gas and Production of Hydrogen or Carbon Monoxide in a Fluidized Bed Using Lattice Oxygen. *Energy Technol.* **2020**, *8*, 1900655.

(20) Chang, H.; Bjørgum, E.; Mihai, O.; Yang, J.; Lein, H. L.; Grande, T.; Raaen, S.; Zhu, Y. A.; Holmen, A.; Chen, D. Effects of Oxygen Mobility in La-Fe-Based Perovskites on the Catalytic Activity and Selectivity of Methane Oxidation. *ACS Catal.* **2020**, *10*, 3707–3719.

(21) Tian, M.; Wang, C.; Han, Y.; Wang, X. Recent Advances of Oxygen Carriers for Chemical Looping Reforming of Methane. *ChemCatChem* **2021**, *13*, 1615–1637.

(22) Iftikhar, S.; Jiang, Q.; Gao, Y.; Liu, J.; Gu, H.; Neal, L.; Li, F. LaNixFe1-XO3−δas a Robust Redox Catalyst for CO2Splitting and Methane Partial Oxidation. *Energy and Fuels* **2021**, *35*, 13921–13929.

(23) Jiang, B.; Li, L.; Zhang, Q.; Ma, J.; Zhang, H.; Yu, K.; Bian, Z.; Zhang, X.; Ma, X.; Tang, D. Iron-Oxygen Covalency in Perovskites to Dominate Syngas Yield in Chemical Looping Partial Oxidation. *J. Mater. Chem. A* **2021**, *9*, 13008–13018.

(24) Gamal, A.; Eid, K.; El-Naas, M. H.; Kumar, D.; Kumar, A. Catalytic Methane Decomposition to Carbon Nanostructures and Cox-Free Hydrogen: A Mini-Review. *Nanomaterials* **2021**, *11*, 10–17.

(25) Li, Y.; Li, D.; Wang, G. Methane Decomposition to COx-Free Hydrogen and Nano-Carbon Material on Group 8-10 Base Metal Catalysts: A Review. *Catal. Today* **2011**, *162*, 1–48.

(26) Amin, A. M.; Croiset, E.; Epling, W. Review of Methane Catalytic Cracking for Hydrogen Production. *Int. J. Hydrogen Energy* **2011**, *36*, 2904–2935.

(27) Sastre, D.; Galván, C. Á.; Pizarro, P.; Coronado, J. M. Enhanced Performance of CH4 Dry Reforming over La0.9Sr0.1FeO3/YSZ under Chemical Looping Conditions. *Fuel* **2022**, *309*, 122122.

(28) Zhang, X.; Pei, C.; Chang, X.; Chen, S.; Liu, R.; Zhao, Z. J.; Mu, R.; Gong, J. FeO6 Octahedral Distortion Activates Lattice Oxygen in Perovskite Ferrite for Methane Partial Oxidation Coupled with CO2 Splitting. *J. Am. Chem. Soc.* **2020**, *142*, 11540–11549.

(29) Yang, J.; Bjørgum, E.; Chang, H.; Zhu, K. K.; Sui, Z. J.; Zhou, X. G.; Holmen, A.; Zhu, Y. A.; Chen, D. On the Ensemble Requirement of Fully Selective Chemical Looping Methane Partial Oxidation over La-Fe-Based Perovskites. *Appl. Catal. B Environ.* **2022**, *301*, 120788.

(30) Yin, X.; Wang, S.; Wang, B.; Shen, L. Perovskite-Type LaMn1−xBxO3+δ (B = Fe, CO and Ni) as Oxygen Carriers for Chemical Looping Steam Methane Reforming. *Chem. Eng. J.* **2021**, *422*, 128751.

(31) Yuan, K.; Zheng, Y.; Li, K.; Yang, Z.; Wang, H.; Wang, Y.; Jiang, L.; Zhu, X.; Wei, Y.; Wang, Y. Enhanced Resistance to Carbon Deposition over La XCe1- XFe XNi1- XO3Oxygen Carrier for Chemical Looping Reforming. *Energy and Fuels* **2021**, *35*, 15867–15878.

(32) Imtiaz, Q.; Yüzbasi, N. S.; Abdala, P. M.; Kierzkowska, A. M.; Van Beek, W.; Broda, M.; Müller, C. R. Development of MgAl2O4-Stabilized, Cu-Doped, Fe2O3-Based Oxygen Carriers for Thermochemical Water-Splitting. *J. Mater. Chem. A* **2015**, *4*, 113–123.

(33) Zhang, L.; Zhang, L.; Hu, Y.; Hu, Y.; Xu, W.; Xu, W.; Huang, C.; Su, Y.; Tian, M.; Zhu, Y.; et al. Anti-Coke BaFe1- XSnxO3-ΔOxygen Carriers for Enhanced Syngas Production via Chemical Looping Partial Oxidation of Methane. *Energy and Fuels* **2020**, *34*, 6991–6998.

(34) Donat, F.; Müller, C. R. CO2-Free Conversion of CH4 to Syngas Using Chemical Looping. *Appl. Catal. B Environ.* **2020**, *278*, 119328.

(35) Luongo, G.; Donat, F.; Müller, C. R. Structural and Thermodynamic Study of Ca A- or Co B-Site Substituted SrFeO3-: δ Perovskites for Low Temperature Chemical Looping Applications. *Phys. Chem. Chem. Phys.* **2020**, *22*, 9272–9282.

(36) Lee, M.; Lim, H. S.; Kim, Y.; Lee, J. W. Enhancement of Highly-Concentrated Hydrogen Productivity in Chemical Looping Steam Methane Reforming Using Fe-Substituted LaCoO3. *Energy Convers. Manag.* **2020**, *207*, 112507.

(37) Masumoto, H.; Watanabe, K. On the Equilibrium Diagram of Co-Fe Binary Alloys. *J. Japan Inst. Met.* **1978**, *42*, 256–260.

(38) Tang, C.; Kousi, K.; Neagu, D.; Metcalfe, I. S. Trends and Prospects of Bimetallic Exsolution. *Chem. - A Eur. J.* **2021**, *27*, 6666–6675.

(39) Bian, Z.; Das, S.; Wai, M. H.; Hongmanorom, P.; Kawi, S. A Review on Bimetallic Nickel-Based Catalysts for CO2 Reforming of Methane. *ChemPhysChem* **2017**, *18*, 3117–3134.

(40) Lai, K. Y.; Manthiram, A. Self-Regenerating Co-Fe Nanoparticles on Perovskite Oxides as a Hydrocarbon Fuel Oxidation Catalyst in Solid Oxide Fuel Cells. *Chem. Mater.* **2018**, *30*, 2515–2525.

(41) Zhang, W.; Wang, H.; Guan, K.; Meng, J.; Wei, Z.; Liu, X.; Meng, J. Enhanced Anode Performance and Coking Resistance by in Situ Exsolved Multiple-Twinned Co-Fe Nanoparticles for Solid Oxide Fuel Cells. *ACS Appl. Mater. Interfaces* **2020**, *12*, 461–473.

(42) Huang, C.; Wu, J.; Chen, Y.-T.; Tian, M.; Rykov, A. I.; Hou, B.; Lin, J.; Chang, C.-R.; Pan, X.; Wang, J.; et al. In Situ Encapsulation of Iron(0) for Solar Thermochemical Syngas Production over Iron-Based Perovskite Material. *Commun. Chem.* **2018**, *1*, 55.